2-1-2001

Diffusion-Reaction-Conduction Processes in Porous Electrodes: The Electrolyte Wedge Problem

Joseph D. Fehribach
Worcester Polytechnic Institute, bach@wpi.edu

Suggested Citation
Fehribach, J. D. (2001). Diffusion-Reaction-Conduction Processes in Porous Electrodes: The Electrolyte Wedge Problem. *European Journal of Applied Mathematics, 12*, 77-96. http://dx.doi.org/10.1017/S0956792501004454

Euro. Jnl of Applied Mathematics (2001), *vol.* 12, *pp.* 77–96. Printed in the United Kingdom

Diffusion-reaction-conduction processes in porous electrodes: the electrolyte wedge problem

J. D. FEHRIBACH†

Department of Mathematical Sciences, Worcester Polytechnic Institute, 100 Institute Rd., Worcester, MA 01609-2247, USA

(*Received 19 June 2000; revised 8 December 2000*)

This work studies mathematical issues associated with steady-state modelling of diffusion-reaction-conduction processes in an electrolyte wedge (meniscus corner) of a current-producing porous electrode. The discussion is applicable to various electrodes where the rate-determining reaction occurs at the electrolyte-solid interface; molten carbonate fuel cell cathodes are used as a specific example. New modelling in terms of component potentials (linear combinations of electrochemical potentials) is shown to be consistent with tradition concentration modelling. The current density is proved to be finite, and asymptotic expressions for both current density and total current are derived for sufficiently small contact angles. Finally, numerical and asymptotic examples are presented to illustrate the strengths and weaknesses of these expressions.

1 Introduction

The *Electrolyte Wedge Problem*, defined by (3.11) and shown schematically in Figure 1, describes in terms of electrochemical potentials the steady-state diffusion-reaction-conduction process associated with the production of current in a wedge of electrolyte in a porous electrode. The domain Ω for this problem is defined to reflect the most interesting portion of many electrodes: a three-phase contact point or meniscus corner. The specific problem motivating the present discussion is the production of current in a Molten Carbonate Fuel-Cell (MCFC) cathode, but the analysis given below is applicable to steady-state current production in any electrode where the three phases (electrolyte, gas and solid electrode) come together to form the sort of wedge depicted in Figure 1, diffusion in the electrolyte is slow, conduction in the solid is (infinitely) fast, and the slowest, rate-determining reaction step occurs at the electrolyte-solid interface.

The importance of such corners or wedges has long been considered. Almost forty years ago, Will [28, 29] presented experimental and theoretical studies of the role of similar corners and their associated thin films for partially immersed platinum electrodes. Bockris & Cahan [3] and Bockris & Srinivasan [4, p. 283] discuss the importance of the contact angle θ_0, and suggest that as much as 99% of the current produced by an electrode may be produced by the 1% of the electrode formed by electrolyte wedges.

† Also at: Laboratory of Materials Science, Technische Universiteit Delft, Rotterdamseweg 137, NL-2628 AL Delft Nederland.

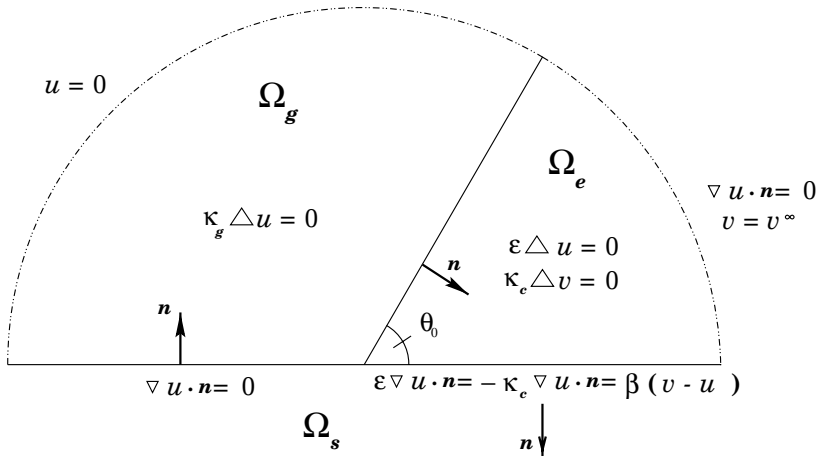

FIGURE 1. Domain $\Omega := \Omega_g \cup \Omega_e$, along with the differential equations and boundary conditions, with notation as in the text. Note the orientation of the unit vectors at the interfaces ($0 < \theta_0 < \pi/2$).

Barendrecht [1, p. 85] attributes the failure of the simple-pore model partially to its failure to take into account these meniscus corners. Such observations are confirmed by more recently MCFC cathode calculations performed for a computational cross-section designed to approximate the cross section shown in Figure 2. This particular MCFC cathode is approximately 64% filled with electrolyte, and there appears to be a wide variety of contact angles for the numerous three-phase contact points. Computations [8] indicate that almost all of the current production in such an MCFC cathode is due to these three-phase contact points[1].

Looking at the notation in Figure 1, let Ω_g denote the gas phase, Ω_e, the electrolyte phase, and Ω_s, the solid phase. The domain for the problem is $\Omega := \Omega_g \cup \Omega_e$. The solid phase (solid electrode) is assumed to be a perfect conductor; thus the potential there is constant, and Ω_s drops out of the domain for the problem. It is also assumed throughout that the contact angle satisfies $\theta_0 < \pi/2$. To produce current, gases diffuse across Ω_g, dissolve/react at $\partial\Omega_{ge}$, diffuse across Ω_e, and finally, react at the $\partial\Omega_{es}$ interface. It is assumed that the slowest reaction step occurs on this interface. Based on these physical and electrochemical processes, one can define two *component potentials*: The first u is the oxidant component potential; it weakly satisfies a Laplace equation inside Ω, so, in particular, u and its normal flux are continuous on $\partial\Omega_{ge}$. The conductivity for the oxidant component, κ_{ox}, is discontinuous at $\partial\Omega_{ge}$:

$$\kappa_{ox} := \begin{cases} \kappa_g & \text{in} \quad \Omega_g \\ \varepsilon & \text{in} \quad \Omega_e \end{cases} \tag{1.1}$$

where $\varepsilon \ll \kappa_g$. The second potential v is the current component potential; it is akin to the electrical potential and is defined only in Ω_e. These potentials are coupled by the single slow reaction at $\partial\Omega_{es}$.

Problems associated with such electrodes have not been studied extensively from a mathematical perspective. In recent years, a number of papers had dealt with the math-

[1] Full-colour current density plots can be viewed at `http://www.wpi.edu/~bach/ECPplots`

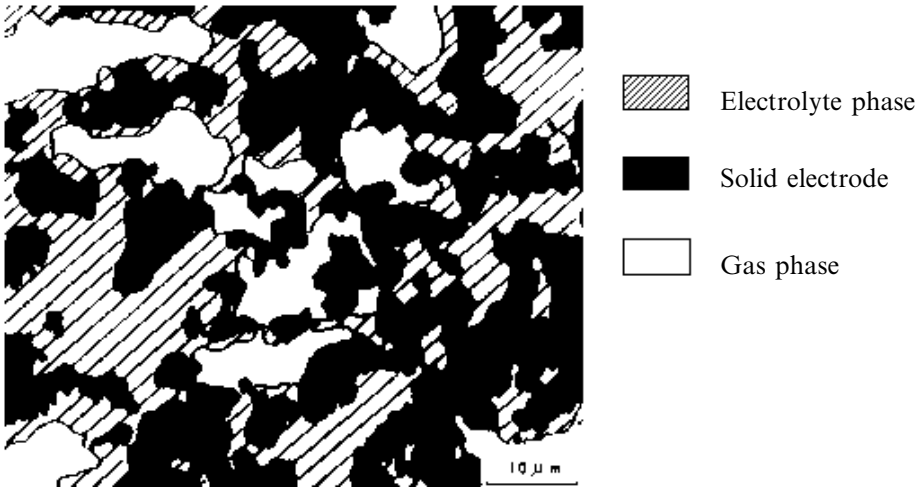

FIGURE 2. Physical electrode cross-section: black-and-white depiction of a colour electron probe microanalysis (EPMA) photograph [27]. Similar cross-sections are discussed in Fontes *et al.* [10]. Approximate dimensions: $70\mu m \times 60\mu m$.

ematical aspects of various other electrode problems, e.g. the Hall effect [15], concentric bipolar electrodes [14], Søderberg electrodes [2] and enzyme electrodes [13]. The mathematical and/or physical issues discussed in each of these works differ significantly from the problem at hand. There is also the well known class of reaction-diffusion problems, but again these are different from the present problem. Only a few mathematical papers have dealt with diffusion-reaction-conduction problems for electrodes: Henderson [12] found an analytic solution for a one-dimensional, time-dependent diffusion-reaction problem modelling a polymer coated electrode. Closer still to the current physical problem is the work of van Duijn & Fehribach [5] who analyzed the agglomerate models of Giner & Hunter [11] (for teflon electrodes) and Yuh & Selman [30] (for MCFC electrodes).

In recent years, component potentials have been introduced to model the electrochemical processes which drive the production of current in porous electrodes; they are related to the concepts of affinities and surface overpotentials. That electrical processes (conduction and reactions) can be described using potential functions is well known; that diffusion can also be described in potential terms is perhaps less known. General discussions of a potential theory for diffusion are given, for example, by Landau & Lifschitz [16, pp. 227–237], or by Robinson & Stokes [25]. These ideas have been extended to porous electrodes, particularly MCFC cathodes, by Fehribach *et al.* [6, 7, 8, 9]. The present paper is divided into seven sections which are more-or-less self-contained, and can be read separately. The next two describe the electrochemical potential modelling used to derive the diffusion-reaction-conduction system (3.11), and thereby show that this system accurately models the physical problem. §2 gives an example of how the component potentials u and v used in (3.11) are defined for MCFC cathodes; the reaction mechanism is assumed to be the peroxide mechanism. Other mechanisms would lead to the same system, but with different coefficients, provided the rate-determining reaction step occurs on $\partial\Omega_{es}$.

The equivalence of the new modelling and the tradition modelling using species concentrations is established in §3. This equivalence is in the sense of *current density equivalence*: the two systems produce the same electrical current along the electrolyte-solid interface. This section also makes clear how much simpler the potential formulation is. The number of dependent variables is reduced from N (depending on the specific process) to two, u and v, and so there are fewer separate equations. In addition, the concentrations must satisfy a nonlinear interface condition on $\partial\Omega_{ge}$ (cf. (3.2)), whereas u weakly satisfies a Laplace equation there. The notation for the potential formulation is also simpler, making it easier to understand the underlying physics and mathematics.

Section 4 deals with the singular nature of the problem in corners where the three phases meet. Indeed at first glance one might expect the current density to be unbounded in such corners, but computations suggest otherwise, and this section establishes the existence of a unique, bounded solution for the Electrolyte Wedge Problem, with a bounded current density, provided that β (the interface reaction rate) is finite.

Next we turn our attention to finding approximate solutions using matched asymptotics. The unusual nature of the matching involving the shifting of the coordinate system makes the analysis of particular interest. An inner solution is given to lowest order in terms of a similarity variable, provided that θ_0 is not too large, and a uniform solution is then derived from the matching. This solution is used to find an approximation for the current density on $\partial\Omega_{es}$, and from it an approximation for the total current produced by the wedge. The final section compares these asymptotic approximations with numerical solutions computed using MATLAB. The comparison indicates how the two very different approximating methods give consistent yet complementary results: the asymptotic results being more accurate than the numerical results when θ_0 is smaller, whereas the numerical results are more accurate when θ_0 is larger.

Finally, a word on the units and notation used in this article is in order: For the asymptotics section below, it is necessary that all the independent variables and coefficients be dimensionless. For the current equivalence section, on the other hand, is is best that the quantities under discussion be associated with their units. In the final discussion, it is also useful not to have eliminated parameters such as v^∞ and β. Therefore, the quantities in (3.11) are in the units typically used in electrochemistry: the electrochemical potentials u and v are in Joule/mole, the conductivities κ_{ox} and κ_c are in $(\Omega\ \mathrm{cm})^{-1}$, the reaction-rate parameter β is in $(\Omega\ \mathrm{cm}^2)^{-1}$, and lengths are in centimeters. However, a separate dimensionless conductivity ϵ is defined and used for the inner solution in the asymptotics section. Regarding notation, the potentials will be denoted by u and v throughout, *except* in the derivations of the component potential. There the electrochemistry tradition of denoting such potentials by μ will be followed, so $u = \mu_{ox}$ and $v = \mu_c$.

2 Component potentials

The definitions for the component potentials for a given reaction mechanism are based directly on the stoichiometry of the mechanism, along with the location of the reaction steps, and which step(s) are rate-determining (slowest). Although the definitions of these potentials could be described abstractly, it is probably clearer to demonstrate the process in terms of a particular example. To be consistent with the Electrolyte Wedge Problem,

our example must have a single rate-determining reaction step on the electrolyte-solid interface $\partial\Omega_{es}$. The one considered here is a version of the peroxide mechanism, one of the primary mechanisms thought to be significant for MCFC cathodes. Definitions for the component potentials for two other mechanisms are considered in Fehribach *et al.* [9], and a detailed discussion of MCFC reaction mechanisms in general is given by Prins-Jansen [21, Ch. 2].

The overall MCFC cathodic reaction is $O_2 + 2CO_2 + 4e^- \rightleftharpoons 2CO_3^=$. The peroxide mechanism achieves this overall reaction through the following sequence of five reaction steps:

$$\begin{array}{lrcl} (a) & CO_2(g) & \rightleftharpoons & CO_2(e), \\ (b) & O_2 + 2CO_3^= & \rightleftharpoons & 2O_2^= + 2CO_2(e), \\ (c) & O_2^= + e^- & \rightleftharpoons & O^= + O^-, \\ (d) & O^- + e^- & \rightleftharpoons & O^=, \\ (e) & O^= + CO_2(e) & \rightleftharpoons & CO_3^=. \end{array} \tag{2.1}$$

Four of these (2.1*b–e*) are electrochemical reactions, while (2.1*a*) denotes the physical dissolution of carbon dioxide as it crosses from the gas into the electrolyte phase. The locations of each of these steps is shown the net-cycle diagram given in Figure 3. Each reaction occurs at one of the five dots in the diagram, and the arrows in the diagram give the forward direction for the mechanism. Current-carriers for the overall mechanism are in boxes, while carbonate ions, $CO_3^=$, which continue from one cycle to the next are circled. Solid vertical lines indicate boundaries between phases. Dots near solid lines indicate interface reactions. The location of each reaction in this schematic follows the description of the mechanism given by Yuh & Selman [30, 31], except for the oxide/carbon-dioxide recombination reaction (2.1*c*). Following more recent work of Lee *et al.* [17], recombination is assumed to occur *in* the electrolyte phase, instead of at the solid-electrolyte interface.

Once the framework of the mechanism is established, one must consider which reactions are rate-determining and which are fast. Again as in Yuh & Selman [30, 31], the peroxide consuming step (2.1*d*) is assumed to be the sole rate-determining step; all other steps are assumed to be relatively fast, and hence approximately in equilibrium. When the entire mechanism is at equilibrium (i.e. when the forward arrows in Figure 3 are exactly balanced by backward arrows in the opposite direction), one can write a sequence of equalities for electrochemical potentials, moving from the oxidant side of Figure 3 across the diagram to the current side:

$$\begin{array}{rcl} \mu_{O_2} + 2\mu_{CO_2(g)} & = & \mu_{O_2} + 2\mu_{CO_2(e)} \\ & = & 2\mu_{O_2^=} - 2\mu_{CO_3^=} + 4\mu_{CO_2(e)} \\ \hline & = & 2\mu_{O^=} + 2\mu_{O^-} - 2\mu_{e^-} - 2\mu_{CO_3^=} + 4\mu_{CO_2(e)} \\ & = & -4\mu_{O^=} - 4\mu_{e^-} - 2\mu_{CO_3^=} + 4\mu_{CO_2(e)} \\ & = & -4\mu_{e^-} + 2\mu_{CO_3^=}. \end{array} \tag{2.2}$$

The dividing line in (2.2) indicates the rate-determining step. So for this version of the

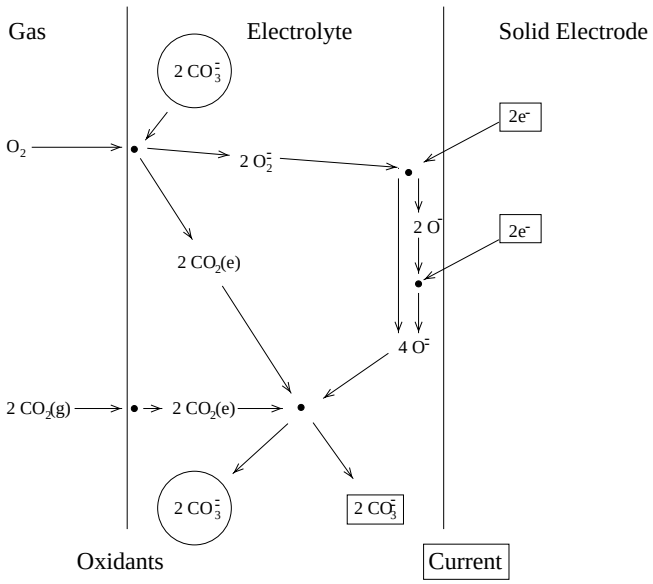

FIGURE 3. Net cycle diagram for the peroxide mechanism: reactions occur at dots, arrows show the forward direction for reactions, solid lines separate phases, current-carriers are in boxes, and carbonate ions which continue from one cycle to the next are circled.

peroxide mechanism, one can define the following *component potentials*:

$$\begin{array}{lllll} u & := & \mu_{ox} & := & \mu_{O_2} + 2\mu_{CO_2(g)} = 2\mu_{O_2^=} - 2\mu_{CO_3^=} + 4\mu_{CO_2(e)}, \\ v & := & \mu_c & := & -4\mu_{e^-} + 2\mu_{CO_3^=}. \end{array} \tag{2.3}$$

Note that the oxidant potential μ_{ox} is defined separately in Ω_g and Ω_e; in each case, the definition is in terms of species present in the given phase, and the two forms are by assumption in equilibrium on $\partial\Omega_{ge}$. The current potential μ_c, on the other hand, is defined simultaneously in terms of species in Ω_e and Ω_s. When the entire mechanism is at equilibrium, $\mu_{ox} = \mu_c$; when the entire mechanism is *not* at equilibrium, these potentials differ because of the rate-determining reaction separating them, and system (3.11) describes how the mechanism proceeds.

3 Current equivalence

This section establishes the equivalence of the current densities produced by the component potential formulation (3.11) and the more-traditional concentration formulation (3.1) and (3.2). The discussion below is sufficiently general to cover a wide range of electrodes and reactions, including MCFC cathodes and the peroxide mechanism discussed above. It assumes that there are N species in Ω_g, N interface conditions on $\partial\Omega_{ge}$, and effectively N species in Ω_e (through the use, where necessary, of equilibrium equations resulting from fast steps in Ω_e). There must be a single rate-determining reaction step at the solid-electrolyte interface $\partial\Omega_{es}$; if two or more reaction steps are simultaneously rate-determining the problem is *not* equivalent to (3.11). The concentration formulation used

by Prins-Jansen *et al.* [22] in their three-phase homogeneous model is of the type being discussed here, as is the system underlying the agglomerate model of Yuh & Selman [30].

For $1 \leqslant k \leqslant N$, the equations in the gas and electrolyte phases are

$$\begin{aligned} \nabla \cdot (D_{k(\mathrm{g})} \nabla c_{k(\mathrm{g})}) &= 0 \quad \text{in } \Omega_g, \\ \nabla \cdot (D_{k(\mathrm{e})} \nabla c_{k(\mathrm{e})}) &= 0 \\ \triangle \phi_e &= 0 \end{aligned} \quad \text{in } \Omega_e, \tag{3.1}$$

where $c_{k(\bullet)}$ is the concentration of the kth species, $D_{k(\bullet)}$ is the associated diffusivity, and ϕ_e is the electrical potential in Ω_e. The Laplace equations for the concentrations in each phase are written separately because they may represent different species, as is the case for the peroxide mechanism above. In terms of concentrations, the interface conditions are of the form

$$\begin{aligned} D_{k(\mathrm{g})} \nabla c_{k(\mathrm{g})} \cdot \mathbf{n} / s_{k(\mathrm{g})} &= D_{k(\mathrm{e})} \nabla c_{k(\mathrm{e})} \cdot \mathbf{n} / s_{k(\mathrm{e})} \\ (c_{k(\mathrm{g})})^{s_{k(\mathrm{g})}} &= H_k \prod_{\ell} (c_{\ell(\mathrm{e})})^{s_{\ell(\mathrm{e})}} \quad \text{on } \partial\Omega_{ge}, \\ \nabla \phi_e \cdot \mathbf{n} &= 0 \\ \nabla c_{k(\mathrm{g})} \cdot \mathbf{n} &= 0 \quad \text{on } \partial\Omega_{sg}, \\ D_{k(\mathrm{e})} \nabla c_{k(\mathrm{e})} \cdot \mathbf{n} &= s_{k(\mathrm{e})} i_F / nF \\ \sigma \nabla \phi_e \cdot \mathbf{n} &= i_F \quad \text{on } \partial\Omega_{es}, \\ c_{k(\mathrm{g})} &= c_{k(\mathrm{g})}^{\mathrm{eq}} \quad \text{on } \partial\Omega_g,\ r = r^{\infty}, \\ \nabla c_{k(\mathrm{g})} \cdot \mathbf{n} &= 0 \\ \phi_e &= \phi_e^{\infty} \end{aligned} \quad \text{on } \partial\Omega_e,\ r = r^{\infty}. \tag{3.2}$$

In (3.2), H_k are appropriate forms of Henry's constant (in the case of CO_2 dissolution) or the equilibrium constant for an electrochemical reaction (in the case of peroxide formulation); $s_{k(\bullet)}$ are the stoichiometric constants for the reaction for the particular species; F is Faraday's constant; and n is the number of electrons involved in the reaction. Fluxes are continuous at $\partial\Omega_{ge}$, but concentrations are not in general. For the second $\partial\Omega_{ge}$ interface condition, not all concentrations are necessarily present in the product; in particular, in the case of CO_2 dissolution, only c_{CO_2} appears of the right-hand side. Although they are far more complicated, the concentration equations in (3.2) on $\partial\Omega_{ge}$ are nothing more than the concentration formulation of the condition that the oxidant potential u weakly satisfies the Laplace equation at this interface.

The Faradaic current density, i_F, on $\partial\Omega_{es}$ is given by the Butler–Volmer equation (e.g. cf. [19]):

$$i_F = i_0 \left[\exp\left(\frac{\alpha_a F}{R_g T} \eta_s \right) - \exp\left(-\frac{\alpha_c F}{R_g T} \eta_s \right) \right], \tag{3.3}$$

where $\eta_s := (v - u)/F$ is known as the *surface overpotential*, R_g is the gas constant,

T is temperature, and α_a and α_c are, respectively, the anodic and cathodic transfer coefficients. To express (3.3) in terms of concentrations, one must have a representation of the electrochemical potentials in terms of concentrations. For minority species in an electrolyte, the ideal gas relation for charged species is normally used:

$$\mu_k = \mu_k^{eq} + R_g T \ln\left(\frac{c_{k(e)}}{c_{k(e)}^{eq}}\right) + r_k F \phi_e, \tag{3.4}$$

where r_k is the charge of the kth species. The reference values $c_{k(e)}^{eq}$ correspond via the conditions to the appropriate far-field gas boundary concentrations. Using the definitions of the component potentials (2.3), this ideal gas relation (3.4) and the Butler–Volmer equation (3.3), one obtains an expression for the Faradaic current density in terms of concentrations and the electrical potential:

$$i_F = i_0 \left[\prod_{k=1}^{N} \left(\frac{c_{k(e)}}{c_{k(e)}^{eq}}\right)^{-p_k} \exp\left(\frac{\alpha_a n F}{R_g T}\eta\right) - \prod_{k=1}^{N} \left(\frac{c_{k(e)}}{c_{k(e)}^{eq}}\right)^{q_k} \exp\left(-\frac{\alpha_c n F}{R_g T}\eta\right) \right], \tag{3.5}$$

where $\eta := \phi_s - \phi_e$ is known as the *overpotential*. The electrical potential ϕ_s is the (constant) potential of the solid electrode Ω_s; it is often arbitrarily set to zero. The powers p_k and q_k, and the transfer coefficients α_a and α_c are determined by the stoichiometry of the reaction mechanism. For many of the reaction mechanisms arising in MCFC cathodes, these are given by Prins-Jansen *et al.* [23]. Equation (3.5) is in fact the more traditional (if also the more complicated) form of the Butler–Volmer equation. For the purposes of the present discussion, only the linear version[2] of the Butler–Volmer equation will be used:

$$i_F = \frac{i_0(\alpha_a + \alpha_c)}{R_g T}(v - u). \tag{3.6}$$

The concentration equations (3.1) and interface conditions on $\partial\Omega_{ge}$ in (3.2) are simply the weak Laplace equation for the oxidant component potential, written in terms of concentrations. Also the boundary conditions in (3.2) on $\partial\Omega_{sg}$ and at $r = r^{\infty}$ match the corresponding conditions in system (3.11). The interesting interface conditions are on $\partial\Omega_{es}$, and these are in fact key to establishing the desired current density equivalence. Indeed that one can reduce the N concentration equations to a single potential equation hinges on the fluxes of each species at $\partial\Omega_{es}$ not being independent, but rather being constrained by the stoichiometry of the rate-determining reaction. This constraint, together with conservation in Ω_e, implies that the fluxes of the species at $\partial\Omega_{ge}$ are also not independent.

To find a consistent definition for ε, the electrochemical conductivity for the oxidant component in the electrolyte phase, recall that the standard definition of the diffusivity of a species in terms of its electrochemical potential is (e.g. cf. Landau & Lifschitz [16,

[2] One could, of course, study the nonlinear version of the Electrolyte Wedge Problem (3.11) by including (3.3), but this would certainly complicate the problem. From a computational point of view, the nonlinear problem is significantly harder to solve, particularly when one wishes to incorporate some form of the electrode geometry as seen in Figure 2. In addition, for many electrodes, $|u - v|/R_g T \ll 1$. This condition is generally valid for MCFC anodes, and often valid for MCFC cathodes (cf. Yuh & Selman [30], particularly the linear experimental/computational anode plots (Figures 6 and 7) and the linear portions near the origin of the cathode plots (Figures 9 and 10)).

pp. 231–232]):

$$D_k := \frac{\kappa_k}{\rho}\frac{\partial \mu_k}{\partial c_k} \tag{3.7}$$

where κ_k is the conductivity of the kth species, ρ is density, and for the moment the phase reference has been dropped to simplify notation. Note that in view of (3.4), one would not expect D_k and κ_k to both simultaneously be constant. The electrochemical flux then equals the standard diffusive flux:

$$\kappa_k \nabla \mu_k = \kappa_k \frac{\partial \mu_k}{\partial c_k}\nabla c_k = \rho D_k \nabla c_k. \tag{3.8}$$

These relations make sense provided the temperature and pressure are approximately constant inside the electrode, and provided each species potential depends only on the concentration of that species (cf. ideal gas representation (3.4)). Along the lines of (3.7) and (3.8), one can use the definition of the oxidant component potential and (3.2) on $\partial\Omega_{es}$ to convert the oxidant flux on $\partial\Omega_{es}$ to a current density:

$$\begin{aligned} \varepsilon \nabla u \cdot \mathbf{n} &= \varepsilon \sum_k s_k \nabla \mu_k \cdot \mathbf{n} \\ &= \varepsilon \sum_k s_k \frac{\partial \mu_k}{\partial c_k}\nabla c_k \cdot \mathbf{n} \\ &= \frac{\varepsilon i_F}{nF}\sum_k \frac{(s_k)^2}{D_k}\frac{\partial \mu_k}{\partial c_k} \\ &= i_F F = \beta(v-u), \end{aligned} \tag{3.9}$$

provided $\beta := i_0(\alpha_a + \alpha_c)F/R_g T$ is the inverse of the charge-transfer resistance, and the oxidant electrochemical conductivity is defined to be

$$\varepsilon := nF^2\left(\sum_k \frac{(s_k)^2}{D_k}\frac{\partial \mu_k}{\partial c_k}\right)^{-1} = nF^2\rho\left(\sum_k \frac{(s_k)^2}{\kappa_k}\right)^{-1}. \tag{3.10}$$

Because the various fluxes must also be proportional on Ω_{ge}, and because the far-field conditions for Ω_g are constant, the same derivation must hold on Ω_{ge}, leading to the same expression (3.10) for κ_g in Ω_g, except that the diffusivities, stoichiometric constants, etc. must now be those for Ω_g. A similar conversion might be expected for the current potential, but it is greatly simplified because the current-carriers (carbonate in the electrolyte, electrons in the solid) are present in excess. So, for example, for the peroxide mechanism, the electrochemical conductivity is essentially the electrical conductivity: $\kappa_c := \sigma/n$.

Relations such as (3.10) are sufficient to establish the current density equivalence of the concentration formulation and the new electrochemical potential formulation shown schematically in Figure 1 and summarized in the following system which defines the

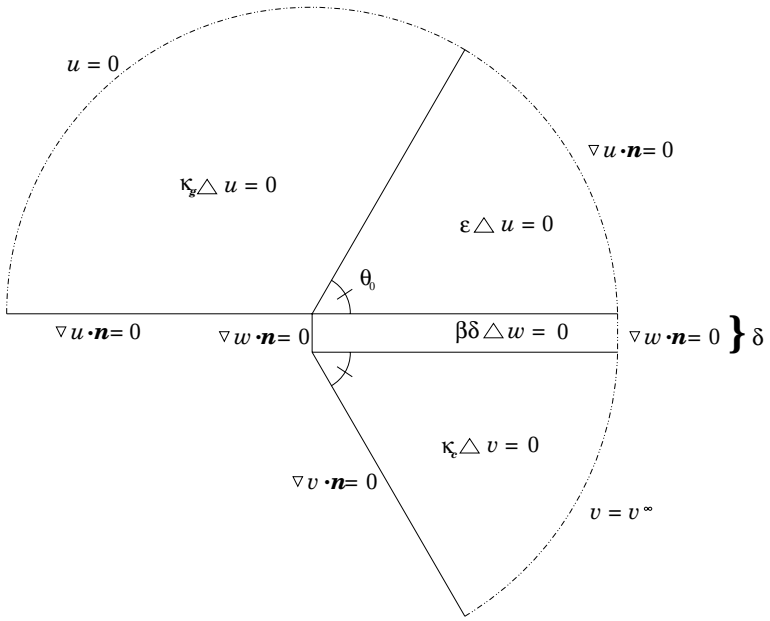

FIGURE 4. Domain for equivalent scalar problem.

Electrolyte Wedge Problem:

$$
\begin{aligned}
&(a) && \nabla\cdot(\kappa_{ox}\nabla u) = 0 && \text{in} \quad \Omega_g \cup \Omega_e,\\
&(b) && \kappa_c \triangle v = 0 && \text{in} \quad \Omega_e,\\
&(c) && \nabla v\cdot\mathbf{n} = \mathbf{0} && \text{on} \quad \partial\Omega_{ge},\\
&(d) && \nabla u\cdot\mathbf{n} = 0 && \text{on} \quad \partial\Omega_{sg},\\
&(e) && \varepsilon\nabla u\cdot\mathbf{n} = -\kappa_c\nabla v\cdot\mathbf{n} = \beta(v-u) && \text{on} \quad \partial\Omega_{es},\\
&(f) && u = 0 && \text{on} \quad \partial\Omega_g,\ r = r^\infty \gg \frac{\varepsilon}{\beta},\\
&(g) && \nabla u\cdot\mathbf{n} = 0;\ v = v^\infty && \text{on} \quad \partial\Omega_e,\ r = r^\infty \gg \frac{\varepsilon}{\beta}.
\end{aligned}
\tag{3.11}
$$

4 Bounded current density

The purpose of this section is to establish the boundedness of the normal derivatives $\partial_n u$ and $\partial_n v$, and hence the current density, along $\partial\Omega_{es}$ for to the Electrolyte Wedge Problem.

Theorem 4.1 *The Electrolyte Wedge Problem* (3.11) *has a unique, bounded solution on the domain* Ω. *Moreover, the normal derivatives* $\partial_n u$ *and* $\partial_n v$ *are bounded along* $\partial\Omega_{es}$.

Proof The proof follows from applying the maximum principle to an equivalent scalar problem. Consider the system of equations defined in Figure 4. The oxidant potential u

is defined in the upper semicircular disk much as it was before; the current potential v is now defined the lower arc wedge which has been 'unfolded' from the original domain. These two portions of the the scalar domain are connected by a rectangular region which is defined based on the reaction that couples these two potentials on the electrolyte-solid interface. Now view the dependent variables (u, v and w) in the various portions of the scalar domain as a single dependent variable, Φ, and assume that Φ and its normal derivative are continuous across each internal boundary in Figure 4. So for all $\delta > 0$, Φ weakly satisfies the Laplace equation. By the maximum principle, the maximum value is $\Phi = u = 0$, and the minimum value is $\Phi = v = v^\infty < 0$, independent of δ, and so the normal fluxes across the rectangular region are bounded by $\beta|v^\infty|$. Taking the limit as $\delta \to 0$, one recovers the boundary condition for the system (note that the diffusion coefficient in the rectangular interface region is proportional to δ). □

5 Matched asymptotics

This section applies the techniques of matched asymptotics to find uniform zeroth order solutions for the Electrolyte Wedge Problem. Because of the nature of the domain, polar as well as Cartesian coordinates will be used. Regarding notation, $F|_a$ on $\partial\Omega_{ab}$ means evaluate F from the a side of the boundary $\partial\Omega_{ab}$.

First, consider the outer solutions ($\varepsilon/\beta \ll r$):

$$\begin{aligned} u(r,\theta,\varepsilon) &= u_0(r,\theta) + \varepsilon u_1(r,\theta) + O(\varepsilon^2), \\ v(r,\theta,\varepsilon) &= v_0(r,\theta) + \varepsilon v_1(r,\theta) + O(\varepsilon^2). \end{aligned} \tag{5.1}$$

Substituting these expansions into system (3.11), one finds that $u_0 = 0$ in Ω_g and $v_0 = v^\infty$ in Ω_e[3]. Both of these solutions depend upon the smallness of the oxidant diffusivity ε in Ω_e: $\kappa_g \partial_n u|_g = \varepsilon \partial_n u|_e$ on $\partial\Omega_{ge}$ implies $\partial_n u_0|_g = 0$, while $\varepsilon \partial_n u|_e = -\kappa_c \partial_n v|_e$ on $\partial\Omega_{es}$ implies $\partial_n v_0|_e = 0$. To find u_0 in Ω_e, observe that $\varepsilon \partial_n u|_e = \beta(v-u)|_e$ on $\partial\Omega_{es}$ implies $u_0|_e = v_0|_e$. On the other hand, u_0 must be continuous across Ω_{ge}. Hence u_0 will depend only upon θ: $u_0(\theta) = v^\infty(\theta_0 - \theta)/\theta_0$ in Ω_e. Notice that the current produced along $\partial\Omega_{es}$ is proportional to $\partial_n u_0|_e = \frac{1}{r}\partial_\theta u_0|_e = -v^\infty/(r\theta_0)$. This is consistent with the singular nature of the problem, but in light of the boundedness proven in the previous section, it is clear that the inner solution ($r \ll \varepsilon/\beta$) cannot have precisely this behaviour.

Turning our attention to the inner solution, let us consider the problem in terms of the inner variables $\mathscr{X} := x/\epsilon$, $\mathscr{Y} := y/\epsilon$ and hence $R := r/\epsilon$. Here the rescaled $\epsilon := \varepsilon/\beta$ has units of length, so the inner variables are unitless. To find a lowest-order representation for the current potential in Ω_e, consider an inner expansion of the form

$$V(R,\theta,\epsilon) = V_0(R',\theta') + \epsilon V_1(R',\theta') + O(\epsilon^2). \tag{5.2}$$

Let $\mathbf{N}$ be the rescaled unit normal: $\mathbf{N} := \mathbf{n}/\epsilon$. Since $\epsilon \partial_N U|_e = -\kappa_c \partial_N V|_e$ along $\partial\Omega_{es}$, and $\partial_N V|_e = 0$ along $\partial\Omega_{ge}$, the only choice for V_0 which is finite at $(X,Y) = (0,0)$ and matches the outer solution is simply $V_0 \equiv v^\infty$. Finding a lowest-order representation for the oxidant potential requires more effort. Indeed a numerical experiment is useful to find

[3] To be exact, the differential equations also allow for radial logarithmic terms, but these would be unbounded near $r = 0$. They must have zero coefficients to match the inner solution in Ω_g and the far-field no-flux condition for u in Ω_e.

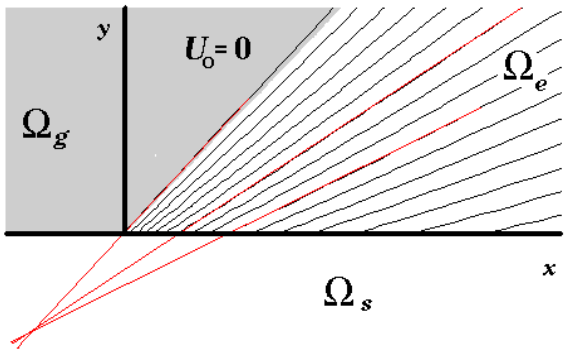

FIGURE 5. Contours for the inner oxidant potential U. Note that $U_0 \equiv 0$ in Ω_g, and appears constant along radial lines in the primed coordinate system. Several of the computed contours have been extended to indicate the common crossing point.

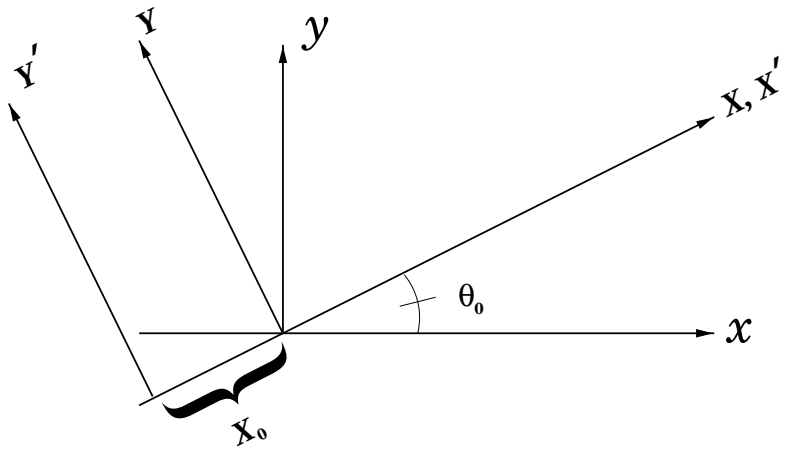

FIGURE 6. Inner coordinate systems: $(\mathscr{X},\mathscr{Y})$ is original; (X,Y) is rotated through θ_0; (X',Y') is rotated through θ_0 and shifted a distance X_0 behind the original origin.

an ansatz for the form of this inner solution. Figure 5 shows level curves for the oxidant potential near the origin, and suggests that one seeks an inner solution U of the form

$$U(R,\theta,\epsilon) = \alpha\theta' + \epsilon U_1(R',\theta') + O(\epsilon^2), \tag{5.3}$$

i.e. $U_0(R',\theta') = U_0(\theta') := \alpha\theta'$ for some constant α. Here the primed coordinate system is rotated and shifted (cf. Figure 6) so that the origin in this system is the point from which the level curves in Figure 5 radiate. Let the primed origin be a distance X_0 behind the original origin along the line $\theta = \theta_0$ ($\theta' = 0$, cf. Figure 6). Note that the shifted angular coordinate θ' is defined in the standard anticlockwise manner with respect to the (X',Y') coordinate system. Figure 6 also defines a third inner coordinate system that will be used below; (X,Y) is rotated, but not shifted.

Now since $U_0 = \alpha\theta'$ satisfies $\triangle U_0 = 0$ in Ω_e, and $U_0 = 0$ on $\partial\Omega_{es}$, we must turn our

attention to $\partial\Omega_{ge}$. To find α, observe that by the chain rule

$$0 = R'\frac{\partial U_0}{\partial R'} = (X + X_0)\frac{\partial U_0}{\partial X} + Y\frac{\partial U_0}{\partial Y} \tag{5.4}$$

while

$$\begin{aligned}\alpha = \frac{\partial U_0}{\partial \theta'} &= \frac{\partial X}{\partial \theta'}\frac{\partial U_0}{\partial X} + \frac{\partial Y}{\partial \theta'}\frac{\partial U_0}{\partial Y} \\ &= -Y\frac{\partial U_0}{\partial X} + (X + X_0)\frac{\partial U_0}{\partial Y} \\ &= \frac{\partial U_0}{\partial \theta} + X_0\frac{\partial U_0}{\partial Y}.\end{aligned} \tag{5.5}$$

An aside is useful here, since the final two lines of (5.5) help one understand in terms of the matching how a nontrivial solution can be bounded: we will find that $X_0 = O(1)$, so that $X_0(\partial_Y U_0)$ is higher-order with respect to the outer solution, and $\partial_\theta U_0$ simply matches $\partial_\theta u_0$. As $(X, Y) \to (0, 0)$, on the other hand, $\partial_X U_0$ and $\partial_Y U_0$ are found to be bounded, so that $|\partial_\theta U_0| \to 0$ and yet $\partial_{\theta'} U_0 \equiv \alpha \to X_0 \partial_Y U_0|_{R'=X_0}$. Returning to the issue of computing α, one can solve equations (5.4) and (5.5) to find expressions for $\partial_X U_0$ and $\partial_Y U_0$. These in turn can be used along with an additional application of the chain rule to find an expression for $\partial_N U_0$ along $\partial_{es}\Omega$ for $R > 0$:

$$\frac{\partial U_0}{\partial \boldsymbol{N}} = \frac{X_0}{(R')^2}\left(\cos\theta_0 + \frac{X_0}{R}\right)\alpha - \frac{\alpha}{R} \tag{5.6}$$

where again, $\boldsymbol{N}$ is the unit normal with respect to the inner coordinates. Recalling that $V_0 = v^\infty + O(\epsilon)$, one finds that the lowest-order boundary condition on $\partial_{es}\Omega$ is $\partial_N U_0 = v^\infty - U_0$. From (5.6), the original ansatz, and since $(R')^2 = R^2 + 2RX_0\cos\theta_0 + X_0^2$ on $\partial_{es}\Omega$, this boundary condition can be written

$$\left(\alpha\theta' - v^\infty\right)(R')^2 = \alpha R + X_0\alpha\cos\theta_0. \tag{5.7}$$

While it is not possible to satisfy this equation exactly, it is possible to find parameter values so that the equation holds approximately for $\theta' \ll 1$, and so that the outer solution is still matched. Specifically, equation (5.7) holds on this interface to first order in θ' provided that

$$\alpha = \frac{-v^\infty X_0}{\cos\theta_0}. \tag{5.8}$$

Finally, as was mentioned above, an expression for X_0 can be found by matching the inner and outer solutions to lowest order. The result is

$$X_0 = \frac{\cos\theta_0}{\theta_0}, \tag{5.9}$$

and since θ' can be written in terms of θ, this yields a uniform lowest-order representation for the oxidant potential:

$$u(r,\theta) = \frac{v^\infty}{\theta_0}\cot^{-1}\left(\frac{\varepsilon X_0}{\beta r}\csc(\theta_0 - \theta) + \cot(\theta_0 - \theta)\right) + O(\epsilon, \theta'^2). \tag{5.10}$$

Note that this representation for u has the correct behaviour for large and small r, and that $u = v^\infty/2$ independent of θ_0 for $R = X_0$, $\theta = 0$ (a point on $\partial\Omega_{es}$).

Of course, the most important quantity to represent is the current density. Although we only have $v = v^\infty + O(\epsilon)$ uniformly throughout Ω_e, equation (3.9) gives an expression for the Faradaic current density on $\partial\Omega_{es}$ which requires only the potentials:

$$\begin{aligned} i_F &= \beta(v-u)/F \\ &= \frac{\beta v^\infty}{F\theta_0}\left[\theta_0 - \tan^{-1}\left(\frac{\tan(\theta_0)}{1+\varepsilon/(\theta_0\beta r)}\right)\right] + O(\epsilon, \theta'^2). \end{aligned} \tag{5.11}$$

Notice that the Faradaic current density approaches a maximum of $\beta v^\infty/F$ near $r = 0$, and decreases rapidly towards zero for $r \gg \varepsilon/\beta$. For $R = X_0$ ($r_{1/2} := \varepsilon X_0/\beta$), the Faradaic current density is halved to $i_F = \beta v^\infty/2F$.

Interestingly, this lowest-order representation for current density (5.11) has an elementary antiderivative:

$$\begin{aligned} \int_0^{r^\infty} i_F dr = \frac{\varepsilon v^\infty}{F\theta_0}\Bigg[& R^\infty\left(\theta_0 - \tan^{-1}\left(\frac{\tan(\theta_0)}{1+1/(\theta_0 R^\infty)}\right)\right) \\ & + \frac{X_0\sin(\theta_0)}{2}\ln\left(\left(\frac{R^\infty}{X_0}\right)^2 + 2R^\infty\theta_0 + 1\right) \\ & - X_0\cos(\theta_0)\left(\theta_0 - \tan^{-1}\left(\frac{\tan(\theta_0)}{1+R^\infty/(X_0\cos(\theta_0))}\right)\right),\Bigg] + O(\epsilon^2, \theta'^2) \end{aligned} \tag{5.12}$$

where $R^\infty := r^\infty\beta/\varepsilon$. Although rather complicated, expression (5.12) essentially gives the total current produced by the electrolyte wedge.

Remarks

(1) One can of course find the first-order solutions u_1, U_1, v_1 and V_1. The solutions v_1 and V_1 and u_1 in Ω_g are all genuinely functions of two variables; there are no easy similarity variables, and thus no easy closed-form representations.

(2) The $O(\theta'^2)$ limitation in (5.11) and (5.12) is not as severe as it might initially appear. Because of (5.7), the requirement that $\theta' \ll 1$ applies only to the inner solution, therefore in (5.10) it means that one must leave the inner solution before θ' becomes large. Because of (5.9), the $O(\theta'^2)$ limitation is really a constraint on the size of θ_0: if θ_0 is sufficiently small, X_0 is is sufficiently large, one enters the outer solution before θ' becomes large. This constraint is demonstrated in the examples in the next section.

(3) Although one might prefer it otherwise, the definitions above imply that both v^∞ and i_F are negative.

6 Numerical and asymptotic examples

This final section presents a comparison of numerical and asymptotic results for the Electrolyte Wedge Problem. In these examples, only the wedge (meniscus) angle θ_0 changes; all of the parameters are fixed. All of the computations discussed here where performed using the 'Adaptive mode' of the MATLAB PDE Toolbox with a 'Relative tolerance' of 5×10^{-9} and the 'longest' refinement method. The number of triangles required for conversion to this tolerance for each example is noted.

For the computations presented below, the parameter values are typical for MCFC cathodes:

- The electrical conductivity σ is assumed to be $1.40\,(\Omega\,\mathrm{cm})^{-1}$, implying that $\kappa_c = 0.350\,(\Omega\,\mathrm{cm})^{-1}$ since $n = 4$.
- A typical far-field electrical potential is $\phi_e^\infty = 70\,\mathrm{mV}$. By combining equations (2.3) and (3.4), one finds that the far-field electrochemical potential for the electrolyte is $v^\infty = 2(-2)F(0.07\,\mathrm{V}) = -27020\,\mathrm{Joule/mole}$.
- With regard to the inverse charge-transfer resistance β (cf. (3.9) and the following text), the temperature is set to $T = 923\,\mathrm{K}$; the gas constant is $R_g = 8.314\,\mathrm{Joule/(mole\,K)}$; and Faraday's constant is $F = 96490\,\mathrm{Coulomb/mole}$. The anodic and cathodic transfer coefficients are, respectively, $\alpha_a = 1.5$ and $\alpha_a = 0.5$, and the exchange current density is given by

$$i_0 \quad = \quad i_0^0 (p_{O_2})^{0.375} (p_{CO_2})^{-1.25}, \tag{6.1}$$

  i_0^0 being the standard exchange current density, and p_X being the partial pressure of species X in the gas phase at 1 atm. (cf. Yuh & Selman [30, p. 2064] or Prins-Jansen *et al.* [23, p. 3588]). Assuming a typical bulk gas concentration of 50% O_2, 10% CO_2, one finds that $i_0^0 = 4\,\mathrm{mA/cm^2}$ [24, p. 3610], and therefore that the exchange current density is 55 $\mathrm{mA/cm^2}$. Hence $\beta = 1.38\,(\Omega\,\mathrm{cm^2})^{-1}$.
- The value of ε comes from (3.10) and the assumption that the minority species in the electrolyte can be treated as ideal gases, so that the relationship between the species potentials and concentrations can be computed using (3.4). The calculation still requires one to estimate the diffusivities of the electrolyte species, and of all the physical parameters needed here, these values are the most difficult to determine accurately. Using $D_{CO_2} = 3.73 \times 10^{-6}\,\mathrm{cm^2/sec}$, $c_{CO_2}^{eq} = 7.145 \times 10^{-7}\,\mathrm{mole/(cm^2\,atm)}$ [20, p. 1197], and $D_{O_2^=} = 1.0 \times 10^{-5}\,\mathrm{cm^2/sec}$ [18], and $c_{O_2^=}^{eq} = 4.08 \times 10^{-7}\,\mathrm{mole/(cm^2\,atm)}$ [26, Table I, with 0.0204 $\mathrm{mole/cm^3}$ as the density of molten carbonate], one finds that $\varepsilon = 6.9 \times 10^{-7}\,(\Omega\,\mathrm{cm})^{-1}$.
- A similar calculation is used to obtain κ_g. Treating both O_2 and CO_2 as ideal gases, one finds that in the gas phase $c_{O_2}^{eq} = 6.6 \times 10^{-6}\,\mathrm{mole/cm^3}$, and $c_{CO_2}^{eq} = 1.32 \times 10^{-6}\,\mathrm{mole/cm^3}$. By taking both diffusivities to be $0.1\,\mathrm{cm^2/sec}$, one then obtains $\kappa_g = 0.15\,(\Omega\,\mathrm{cm})^{-1}$.
- Finally, the domain radius r^∞ is taken to be $1\,\mu\mathrm{m}$ (so $R^\infty = r^\infty \beta/\varepsilon = 200$). This radius is consistent with the pore size seen in Figure 2.

A summary of the results for three values of θ_0 ($\pi/18$, $\pi/10$ and $\pi/4$) are displayed in the tables below. The total current I produced by the wedge is defined to be the integral of the current density multiplied by a typical wedge thickness (perpendicular to the cross-section). Here the wedge thickness is assumed to be $10\,\mu\mathrm{m}$. The asymptotic values were computed using expressions from §5 (cf. equation (5.9), (3.9) and (5.12)). The numerical values for the total current I are based a trapezoidal rule integration along $\partial\Omega_{es}$ of the current density i_F computed by MATLAB. The numerical values for $i_F(0)$ were found using a three-point boundary interpolation: $i_F(0) = i_F(3x) + 3(i_F(x) - i_F(2x))$ where x is the grid spacing along $\partial\Omega_{es}$, and those for $r_{1/2}$ were found using a linear interpolation. Finally, the numerical values for X_0 were measured directly from plots similar to Figure 5; the

Table 1. *Comparison for* $\theta_0 = \pi/18$ (*number of triangles: 29362*)

	Numerical value	Asymptotic value
X_0	5.5 – 5.7	5.6
$r_{1/2}$	0.030 μm	0.029 μm
$\lvert i_F(0)\rvert$	385 mA/cm^2	386 mA/cm^2
$\lvert I\rvert$	0.0041 μA	0.0039 μA

Table 2. *Comparison for* $\theta_0 = \pi/10$ (*number of triangles: 20213*)

	Numerical value	Asymptotic value
X_0	3.1 – 3.2	3.0
$r_{1/2}$	0.017 μm	0.015 μm
$\lvert i_F(0)\rvert$	384 mA/cm^2	386 mA/cm^2
$\lvert I\rvert$	0.0027 μA	0.0024 μA

Table 3. *Comparison for* $\theta_0 = \pi/4$ (*number of triangles: 12112*)

	Numerical value	Asymptotic value
X_0	1.1 – 1.2	0.90
$r_{1/2}$	0.0071 μm	0.0045 μm
$\lvert i_F(0)\rvert$	373 mA/cm^2	386 mA/cm^2
$\lvert I\rvert$	0.0013 μA	0.00088 μA

uncertainties in these measurements reflect the difficulty in making these measurements (see Tables 1–3).

The summary indicates how similar the numerical and asymptotic results, particularly for small θ_0. Based on the asymptotic derivation in the previous section, one would expect the numerical values to be more accurate for large θ_0. For small θ_0, more-careful consideration of the results is needed to determine which values are more accurate. The differences between the numerical and asymptotic approaches can also be seen by considering plots of the current density i_F along $\partial\Omega_{es}$ shown in Figures 7 and 8.

As expected, the numerical and asymptotic current density plots are more consistent for $\theta_0 = \pi/18$ than for $\theta_0 = \pi/4$. Deficiencies in the numerical solution, however, can be seen by 'zooming in' on the plot in Figure 7; such an enlargement is seen in Figure 9. While it is probably possible to find or write a numerical solver that handles the small θ_0 cases better than MATLAB, it should be noted that this difficulty is inherent, at least to finite-element methods. Any finite-element solver will work less well as $\theta_0 \searrow 0$.

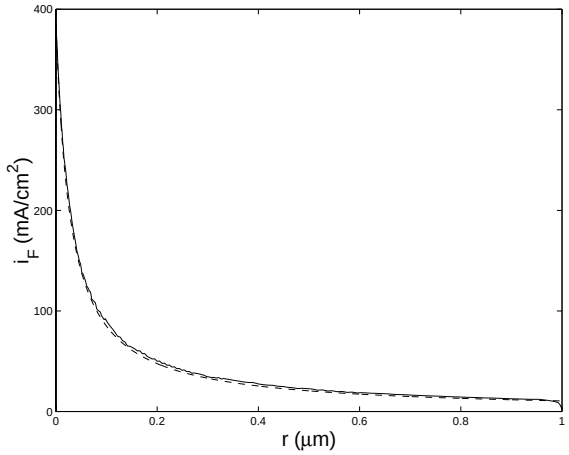

FIGURE 7. Comparison of numerical (solid) and asymptotic (dashed) current density for $\theta_0 = \pi/18$.

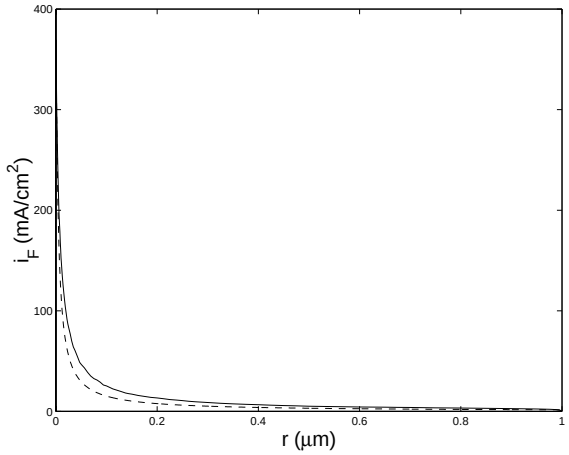

FIGURE 8. Comparison of numerical (solid) and asymptotic (dashed) current density for $\theta_0 = \pi/4$.

7 Conclusions

The work presented here deals with the current density and total current produced by a wedge of electrolyte (meniscus corner) inside a porous electrode. Such wedges are known to be a significant source of the current produced by many electrodes. A new formulation (the Electrolyte Wedge Problem) in terms of electrochemical component potentials is shown to be equivalent to the traditional concentration formulation, and then used to show that the steady-state current densities associated with electrolyte wedges are finite, and to compute these current densities. With the current density profiles in hand, it is easy to compute the total steady-state current produced by the wedge.

The main advantage of the component-potential approach is that it simplifies both the analysis and the computations. It would be significantly more difficult to approximate the current densities, or to establish their boundedness, if one had to think in terms

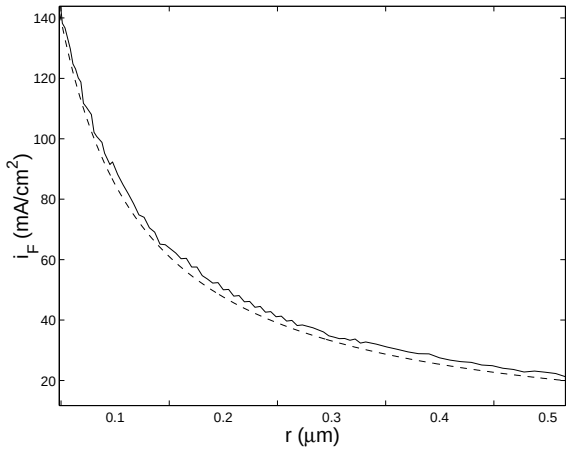

FIGURE 9. Zoom-in comparison of numerical (solid) and asymptotic (dashed) current density for $\theta_0 = \pi/18$. Note jaggedness of numerical current density.

of concentrations. The component potentials, at least for the steady-state, organize the physics and electrochemistry of the problem in an effective manner.

It is also impressive that two very different approaches for computing the current densities give such consistent results: the numerical methods know nothing about the existence of X_0 or the matching, while the asymptotic methods know none of the finite-element theory underlying the numerical computations. Still, the above calculations suggest that the asymptotic approach is only useful for $\theta_0 \geqslant \pi/4$ as a rough indicator of the current and the associate parameters; traditional numerical computations are required to find more accurate representations. For small θ_0, on the other hand, the asymptotic approach is far superior to the numerical approach since it even yields a closed-form representation (5.12) for the total current produced on $\partial\Omega_{es}$, and avoids the jaggedness seen in Figure 9. One can imagine a mixed asymptotic/numeric scheme, a sort of domain decomposition, which uses one approach for small θ_0 and the other approach for larger θ_0.

Acknowledgements

Partially supported by the National Science Foundation under grant DMS-9501022 and NWO (Nederlandse Organisatie voor Wetenschappelijk Onderzoek) under the bezoekersbeurs B 74-48.

References

[1] BARENDRECHT, E. (1993) Electrochemistry of fuel cells. In: L. J. M. J. Blomen and M. N. Mugerwa, editors, *Fuel Cell Systems*. Plenum.

[2] BERMÚDEZ, A. & MUÑOZ-SOLA, R. (1999) Existence of solutions of a coupled problem arising in the thermoelectrical simulation of electrodes. *Quart. Appl. Math.* **57**, 621–636.

[3] BOCKRIS, J. O'M. & CAHAN, B. (1969) Effect of finite contact angle meniscus on kinetics in porous electrodes. *J. Chem. Phys.* **50**, 1307.

[4] BOCKRIS, J. O'M. & SRINIVASAN, S. (1993) *Fuel Cells: Their Electrochemistry*. McGraw-Hill.

[5] van Duijn, C. J. & Fehribach, J. D. (1993) Analysis for a molten carbonate fuel cell. *Electr. J. Diff. Eqns.* **6**, 1–25.

[6] Fehribach, J. D., Prins-Jansen, J. A., Hemmes, K. & de Wit, J. H. W. (1997) Internal resistance computations for MCFC using electrochemical potentials. In: J. R. Selman, I. Uchida, H. Wendt, D. A. Shores and T. F. Fuller, editors, *Proc. 4th Int. Symposium of Carbonate Fuel Cell Technology*, **PV 97-4**, pp. 362–369.

[7] Fehribach, J. D., Prins-Jansen, J. A., Hemmes, K. & de Wit, J. H. W. (1998) The modeling of molten carbonate fuel-cell cathodes using electrochemical potentials. *Proc. 5th International Symposium on Molten Salt Chemistry and Technology*, pp. 123–126.

[8] Fehribach, J. D., Prins-Jansen, J. A., Hemmes, K., de Wit, J. H. W. & Call, F. W. (2001) On modeling molten carbonate fuel-cell cathodes by electrochemical potentials. *J. Appl. Electrochem.* **30**, 1015–1021.

[9] Fehribach, J. D., Prins-Jansen, J. A., Hemmes, K., de Wit, J. H. W. & Call, F. W. (1998) *The derivation of electrochemical-potential models for molten carbonate fuel-cell cathodes.* WPI Mathematical Sciences Preprints **MS-01-98-03**, pp. 1–24.

[10] Fontes, E., Lagergren, C. & Simonsson, D. (1993) Mathematical modelling of the MCFC cathodes. *Electrochem. Acta*, **38**, 2669–2682.

[11] Giner, J. & Hunter, C. (1969) The mechanism of operation of the teflon-bonded gas diffusion electrode: A mathematical model. *J. Electrochem. Soc.* **116**, 1124–1130.

[12] Henderson, D. (1980) An analytical solution of a boundary value problem describing a reversible electrochemical reaction at a polymer coated electrode. *Utilitas Math.* **17**, 231–238.

[13] Jochum, P. (1983) The numerical treatment of a two-phase model for enzyme electrodes. In: B. Brosowski and E. Martensen, editors, *Approximation and Optimization in Mathematical Physics.* Verlag Peter Lang, pp. 35–51.

[14] Johnston, P. R. & Kilpatrick, D. (1999) An asymptotic estimate for the effective radius of a concentric bipolar electrode. *Math. Biosci.* **161**, 65–82.

[15] Krutitskii, P. A. (1998) On the electric current from electrodes in a magnetized semiconductor film. *IMA J. Appl. Math.* **60**, 285–297.

[16] Landau, L. D. & Lifshitz, E. M. (1987) *Fluid Mechanics* (*2nd ed.*). Pergamon.

[17] Lee, G. L., Selman, J. R. & Plomp, L. (1993) Comparison of MCFC cathode materials by porous electrode performance modeling. *J. Electrochem. Soc.* **140**, 390–396.

[18] Moutiers, G., Cassir, M. & Devynck, J. (1992) Oxygen reduced species in molten Li_2CO_3-K_2CO_3 (42.7+57.3 mol-percent) at 650C – a thermodynamic, voltammetric and convolution potential sweep characterization. *J. Electroanal. Chem.* **324**, 175–189.

[19] Newman, J. S. (1991) *Electrochemical Systems* (*2nd ed.*). Prentice Hall.

[20] Nishina, T., Uchida, I. & Selman, J. R. (1994) Gas electrode reactions in molten carbonate media, part V. *J. Electrochem. Soc.* **141**, 1191–1198.

[21] Prins-Jansen, J. A. (1996) *Cathodes in molten carbonate fuel cells, mathematical modeling and experimental characterization.* PhD thesis, Technische Universiteit Delft, The Netherlands.

[22] Prins-Jansen, J. A., Fehribach, J. D., Hemmes, K. & de Wit, J. H. W. (1996) A three-phase homogeneous model for porous electrodes in molten carbonate fuel cells. *J. Electrochem. Soc.* **143**, 1617–1628.

[23] Prins-Jansen, J. A., Hemmes, K. & de Wit, J. H. W. (1997) An extensive treatment of the agglomerate model for porous electrodes in molten carbonate fuel cells Part I: Qualitative analysis of the steady-state model. *Electrochimica Acta*, **42**, 3585–3600.

[24] Prins-Jansen, J. A., Hemmes, K. & de Wit, J. H. W. (1997) An extensive treatment of the agglomerate model for porous electrodes in molten carbonate fuel cells Part II: Quantitative analysis of time-dependent and steady-state model. *Electrochimica Acta*, **42**, 3601–3618.

[25] Robinson, R. A. & Stokes, R. H. (1959) *Electrolyte Solutions* (*2nd ed.*). Butterworths.

[26] Smith, S. W., Vogel, W. M. & Kapelner, S. (1982) Solubilities of oxygen in fused Li_2CO_3-K_2CO_3. *J. Electrochem. Soc.* **129**, 1668–1670.

[27] Takashima, T., Ohtsuka, K., Kobayashi, N. & Fujimura, H. (1990) Stack performance model

of molten carbonate fuel cell. In: J. R. Selman, D. A. Shores, H. C. Maru and I. Uchida, editors, *Proc. 2nd Symposium on Molten Carbonate Fuel Cell Technology*, **PV 90-16**, 378–394.

[28] Will, F. G. (1963) Electrochemical oxidation of hydrogen on partially immersed platinum electrodes, I. Experiments and interpretation. *J. Electrochem. Soc.* **110**, 145–151.

[29] Will, F. G. (1963) Electrochemical oxidation of hydrogen on partially immersed platinum electrodes, II. Theoretical treatment. *J. Electrochem. Soc.* **110**, 152–160.

[30] Yuh, C. Y. & Selman, J. R. (1984) Polarization of the molten carbonate fuel cell anode and cathode. *J. Electrochem. Soc.* **131**, 2062–2069.

[31] Yuh, C. Y. & Selman, J. R. (1992) Porous-electrode modeling of the molten-carbonate fuel-cell electrodes. *J. Electrochem. Soc.* **139**, 1373–1379.